ADVANCED MATERIALS TECHNOLOGIES

Supporting Information

for *Adv. Mater. Technol.,* DOI: 10.1002/admt.202001307

Vancomycin-Loaded Microneedle Arrays against Methicillin-Resistant *Staphylococcus Aureus* Skin Infections

*Jill Ziesmer, Poojabahen Tajpara, Nele-Johanna Hempel, Marcus Ehrström, Keira Melican, Liv Eidsmo, and Georgios A. Sotiriou**

Supporting Information

Vancomycin-Loaded Microneedle Arrays Against Methicillin-Resistant Staphylococcus Aureus Skin Infections

*Jill Ziesmer, Poojabahen Tajpara, Nele-Johanna Hempel, Marcus Ehrström, Keira Melican, Liv Eidsmo, Georgios A. Sotiriou**

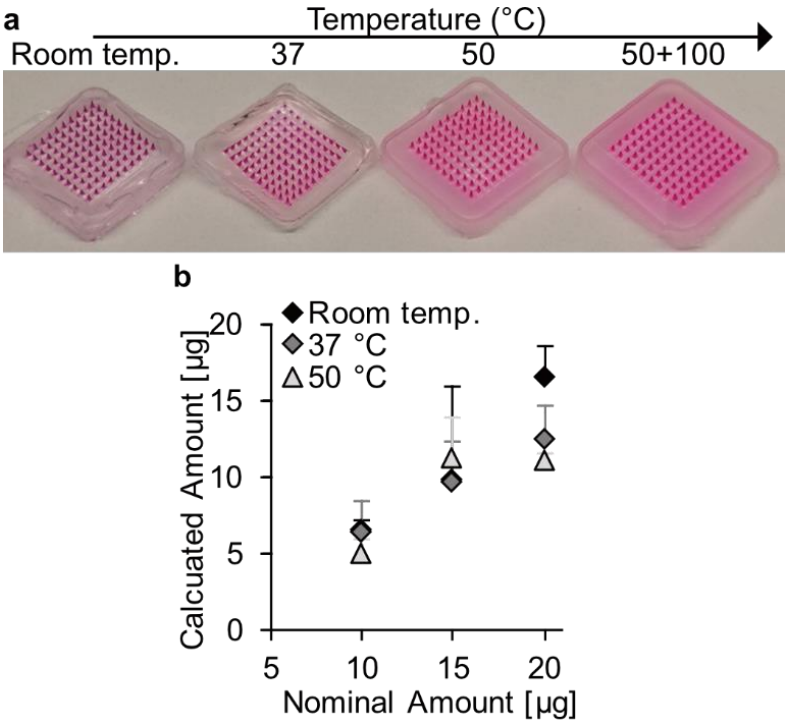

Figure S1: Temperature influence in loading in MN tips with water-insoluble backing layer. (a) Digital images of MN arrays loaded with 10 µg SR. The PMMA support layer was dried at different temperatures. (b) Measured VAN concentration against nominal loaded amount depending on different drying temperatures, n=3.

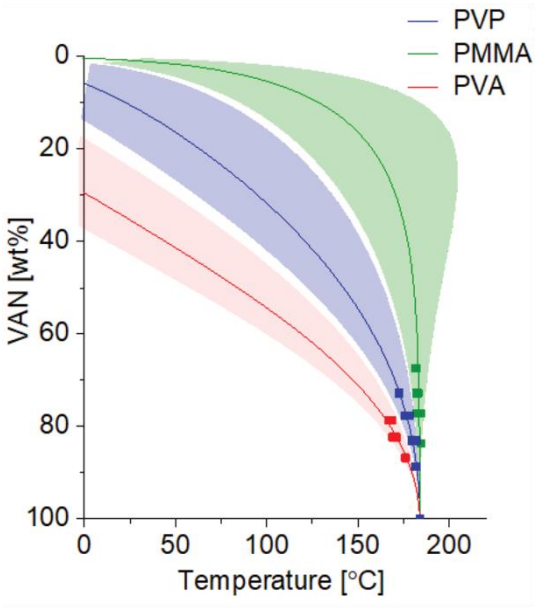

Figure S2: Results from DSC VAN solubility measurements in different polymers. VAN has an estimated solubility at room temperature of 35 wt% ($t_{2.5}$ = 24 wt%, $t_{97.5}$ = 43 wt%), 10 wt% ($t_{2.5}$ = 3 wt%, $t_{97.5}$ = 20 wt%), and 1 wt% ($t_{2.5}$ = 0 wt%, $t_{97.5}$ = 3 wt%) in PVA, PVP, and PMMA, respectively. Single data points with predicted model and respective SD are plotted for n=2.

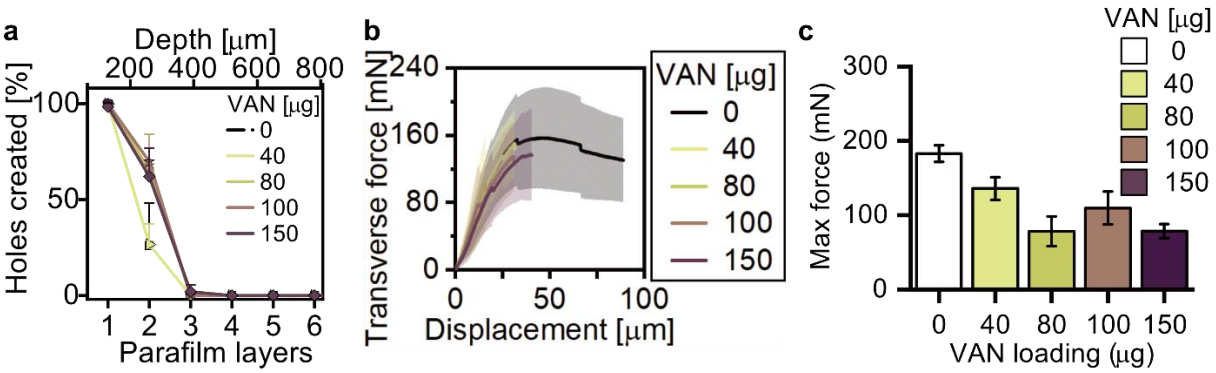

Figure S3: (a) Insertion depth of VAN-loaded MN arrays into eight stacked layers of parafilm as a skin model utilizing a spring applicator at 1.6 N force, n=3. (b) Transverse force as a function of displacement curves of needles at different VAN concentrations, n=9. (c) Maximum transverse force applied before needle failure for PMMA core only (after dissolution of water-soluble, VAN-loaded tip), n=3.

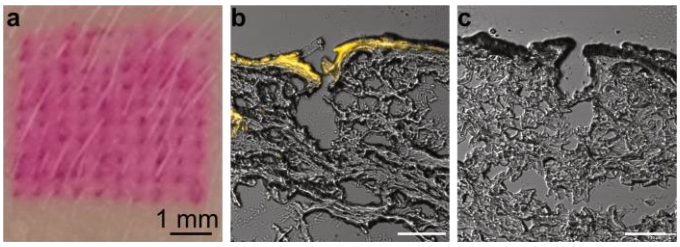

Figure S4: Insertion of PVA/PMMA MN arrays into thawed pork using a spring applicator. (a) Top-view digital images skin after insertion of SR-loaded MN arrays. (b) Fluorescence and bright field overlay micrograph of histological section of skin after SR-loaded MN array insertion. (c) Bright field micrograph of skin section after insertion of 100 µg VAN-MN array insertion.

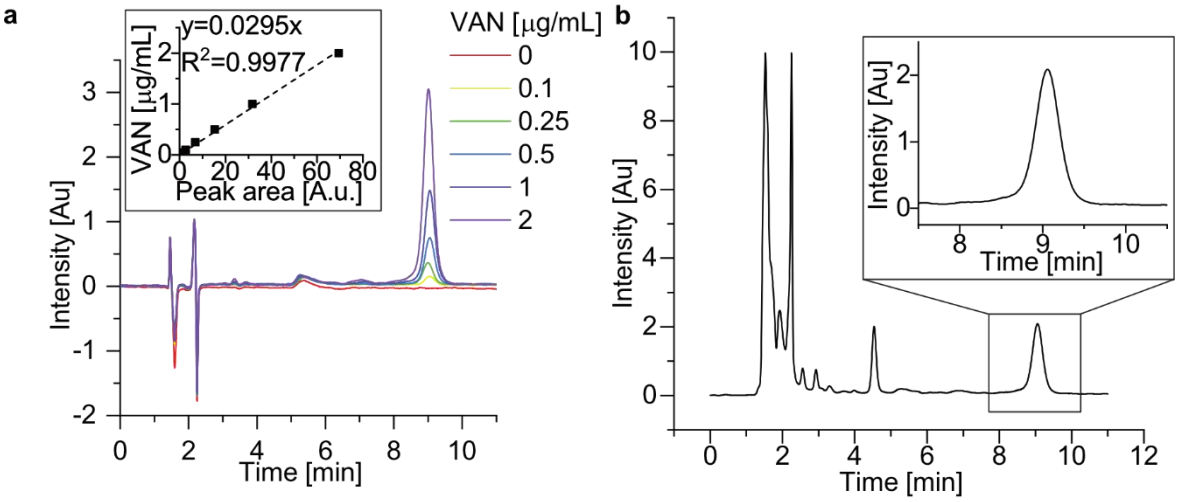

Figure S5: Chromatograms of HPLC analysis of VAN. (a) Chromatograms of VAN standards diluted in PBS at 0-2 µg mL^{-1}, VAN eluting at around 9 min, insert shows linearity between VAN concentration and peak area. (b) Example chromatogram of one tissue sample, insert shows enlarged VAN peak.

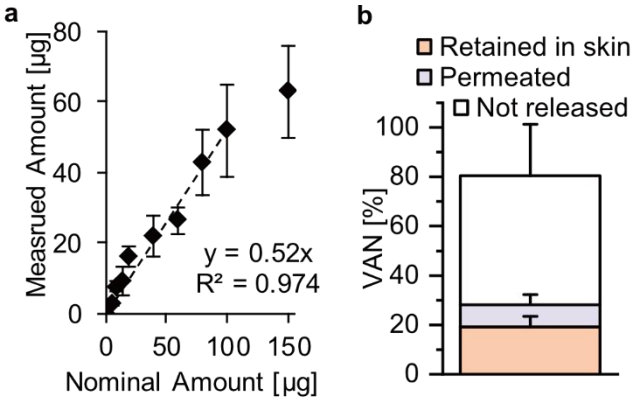

Figure S6: Calculation of relative MN content and skin delivery. (a) Measured VAN concentration against nominal loaded amount, n=6. (b) Relative VAN measured after termination of Franz experiment in the skin (retained), in the receptor chamber (permeated) or within the removed arrays (not released) for 10 min MN application, n=6.

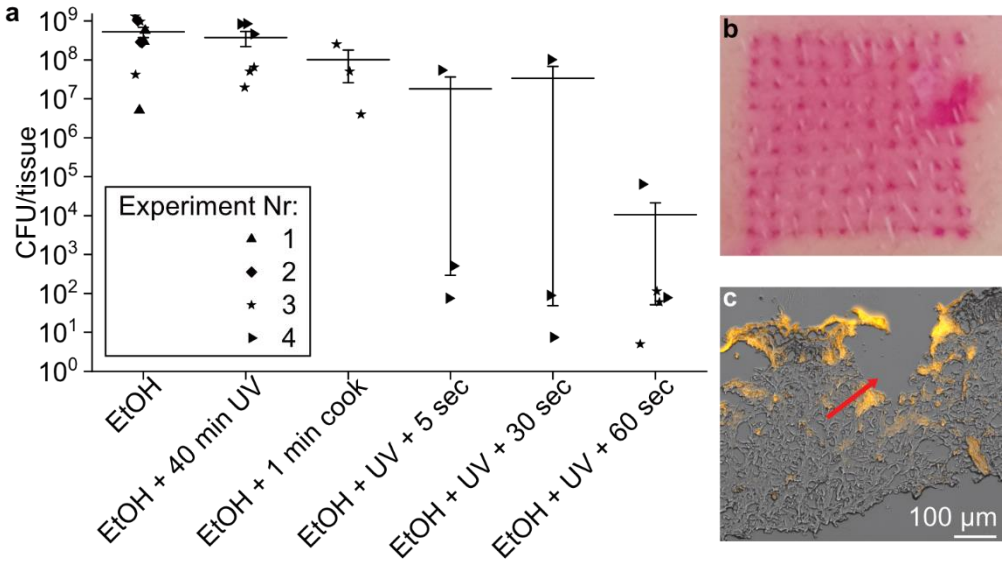

Figure S7: Effects of disinfection methods on CFU count. (a) CFU counts on lysogeny broth agar of porcine skin homogenates after different disinfection routines (soaking in 20 min EtOH, UV irradiation, cooking in water at 95 °C for different lengths). (b) Insertion of SR loaded MN arrays into porcine skin disinfected with EtOH, UV radiation and one minute of cooking. Digital top-view image (b) and tissue sectioning (c) shows successful needle insertion but reveals disintegration of skin tissue causing crater-like insertion holes from needles (red arrow).

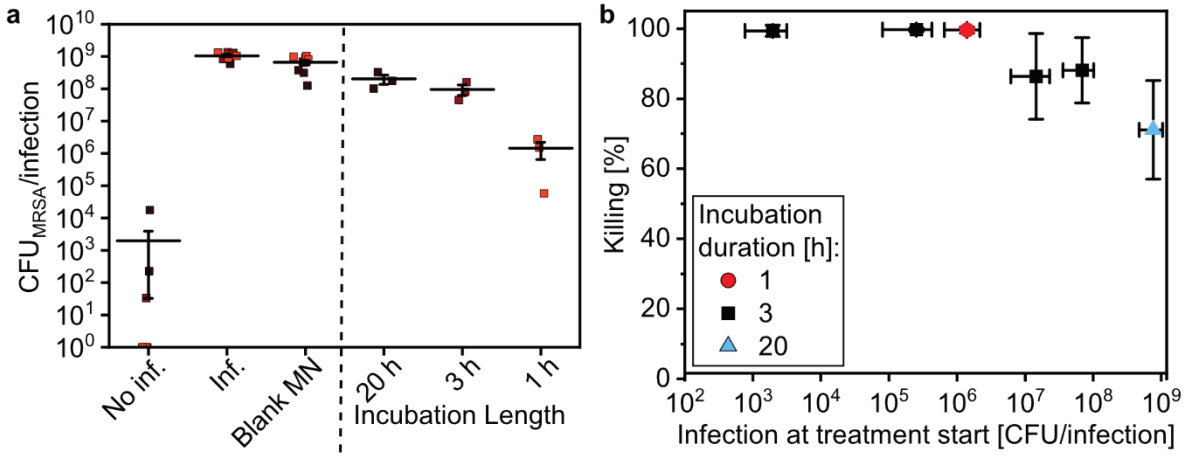

Figure S8: a) Effect of 4 x VAN-MN application on the reduction of MRSA in ex vivo porcine skin model. First MN array application was conducted after varying incubation lengths (20, 3, or 1 h). Total counted MRSA CFU are plotted, zero CFU are plotted as one CFU for visualization in the log-scale. Averages of three technical replicates with SE of the mean are plotted. b) Percentage killing (calculated against infection controls of treatment groups) in dependence of bacterial burden at point of treatment start, n=3.